Korean J. Chem. Eng., 39(2), 377-388 (2022)
DOI: 10.1007/s11814-021-0917-y

pISSN: 0256-1115
eISSN: 1975-7220

Synthesis and characterization of cross linked N-methylene phosphonic chitosan resin chelated with Al(III) for use as adsorbent for fluoride removal from aqueous solutions

Junyu Fan*, Longhua Yu, Xin Zhou*, and Jie Liu*,†**

*Department of Military Facilities, Army Logistics Academy, Chongqing, 401311, China
**School of Environmental Science and Engineering, Hunan University, Changsha, 410082, China
(*Received 3 June 2021 • Revised 27 July 2021 • Accepted 3 August 2021*)

Abstract−Excessive fluoride in groundwater is becoming a worldwide environmental problem increasing the risk of fluorosis. In this study, an eco-friendly new defluorination resin (Al-CPCM) was synthesized by a modified emulsion method. The skeleton of the resin is cross-linked N-methylene phosphonic chitosan and the incorporated Al(III) is the binding site of fluoride. The batch experiments conducted using pure synthetic sodium fluoride solutions showed that Al-CPCM exhibited a fast fluoride removal within 30 min, maintained stability from pH 3-10. Effect of presence of other anions was studied by adding one extra anion at a time and it was observed that presence of phosphate and carbonate ions significantly degraded the adsorption capacity of the resin. The maximum adsorption capacity was 15.067 mg/g at 30 °C and the adsorption behavior was well-fitted with the pseudo-second-order kinetic model and Hill isotherm model. The results of *in-situ* flow ATR-FTIR and thermodynamics studies show that the fluoride adsorption dominantly implemented by ion exchange with surface hydroxyl of chelated Al^{3+} in the resin. In addition, the adsorption capacity only decreased by 5.5% after six successive sorption/desorption cycles, indicating a better regeneration efficiency among other defluorinated resins. Finally, a column experiment was performed using ground water and, in this case, it is observed that the adsorption capacity of the resin was much lower and the decrease in adsorption capacity after elution/regeneration is was larger (both mainly due to the presence of alternate anions/cations in the feed solution). More elaborate column experiments with real-life groundwater samples are required to assess the suitability of the proposed resin for use as a commercial adsorbent.

Keywords: Chitosan, Amino-methyl Phosphonic Resin, Aluminum Complex, Emulsion Polymerization, Defluorination

INTRODUCTION

Fluorine pollution in groundwater has gradually become a common crisis in recent years for groundwater used as drinking water. The excessive fluorine is from the dissolution of fluorine-containing minerals and industrial production. In some areas of the world, the fluoride content in groundwater has been found to exceed the 1.5 mg/L allowable limit set by the WHO and BIS several times [1-3]. Long-term intake of high levels of fluoride will greatly increase the risk of fluorosis [4-6], causing damage to teeth and bones. Thus, this higher concentration of fluoride needs as a contaminant to be removed in time.

Special fluorine removal resin is an effective defluorination technology to separate excess fluoride in water, which is generally made of cationic chelating resins by chelating polyvalent metal ions on themselves [7,8]. The principle of fluorine removal using resin is based on the hard-soft-acid-base (SHAB) theory, which shows that the strongly hydrated fluoride anions easily combine with the harder polyvalent metal ions, such as Al(III), Fe(III), La(III), Ce(IV), Ti(IV) and Zr(IV). Among these, Al(III) has become the first choice for resin loading due to its comprehensive advantages in performance and cost [9].

In addition to the loaded metals, defluorination performance of the resin is also related to the chelating group. At present, sulfonated monophosphonic acid group, iminodiacetic acid group and methyl phosphonic acid group are most commonly used in commercial resins [9-11]. The resins are prepared by grafting these functional chains on the polymer framework, such as the most widely used polyacrylic acid and polystyrene [12-14]. These common polymers have good chemical stability, ensuring a sufficient strength for resin. But in fact most of them are non-degradable in the natural environment, and their synthesis from monomers is not environmentally friendly either [15,16].

As a kind of biomass extracted from shells, chitosan is non-toxic, biodegradable and easily available. The resin cross-linked or polymerized with chitosan as the monomer not only exhibits excellent physical and chemical properties, but also can overcome those complications of common polymers [17,18]. Due to the amino and hydroxyl groups in the structure of chitosan, the polyvalent metal ions can be directly chelated on the cross-linked chitosan and then can be used as a fluorine removal resin [19,20]. However, inhibited by the steric hindrance of the glycoside ring, its amount of metal loaded is inferior to most commercial resins, unless more chelating groups are grafted [21]. Actually, it is feasible to graft other side chains with the amino group on chitosan through Schiff base reaction [22]. Thus in this study, a cross-linked N-methylene phosphonic chitosan microspheres was synthesized and chelated with Al(III) to be a new fluorine removal resin. The removal per-

†To whom correspondence should be addressed.
E-mail: liujiely@hotmail.com

formance and mechanism of the resin were investigated and discussed. And to the best of our knowledge, such research has not been reported yet.

MATERIALS AND METHODS

1. Materials

Chitosan powder, with a degree of deacetylation of 85% and average molecular weight of 48,000 g/mol, liquid paraffin, ethyl acetate and Tween 80 were from Sinopharm Chemical Reagent Co., Ltd. (Shanghai, China). Epichlorohydrin, dimethyl phosphate and petroleum ether were supplied by Macklin Biochemical Co., Ltd (Shanghai, China). Formaldehyde solution (36.8-38%) was purchased from Sigma-Aldrich Chemical Inc. (Saint Louis, USA). The total ionic strength regulator for fluoride electrode method (TISAB II) was by Thermo Scientific (Waltham, USA). Other reagents used in this study, including $Al_2(SO_4)_3{\cdot}18H_2O$, NaOH, HCl, NaCl and NaF were obtained from Sinopharm Chemical Reagent. And all the chemicals were analytical or higher grade and utilized directly without further purification.

2. Synthesis of the CPCM and Al-CPCM

The synthesis scheme of Al-CPCM is displayed in Fig. 1. About 5 g of the chitosan was dissolved in 90 mL of 1% acetic acid (v/v) solution. Then 10 mL of 3 mol/L dimethyl phosphate was added to it with stirring. Almost an hour later at room temperature, this solution was heated to 70 °C and kept for 30 min after being added dropwise with 5 mL of formaldehyde solution. Then, stirring was continued followed by addition of 150 mL of liquid paraffin, 10 mL of ethyl acetate and 4 mL of Tween 80 to ensure emulsification and pore formation. After 20 min, the crosslinking agent epichlorohydrin (5 mL) was injected into the resultant dispersion and its alkalinity was adjusted to pH 10 drop by drop with 1 mol/L sodium hydroxide through a burette 30 min later. The shaped resin beads could be obtained 2 hours later after separated and washed with petroleum ether and DI water alternately. This was the cross-linked N-methylene phosphonic chitosan microspheres, labeled as CPCM. Analogously, the beads synthesized by the same process except replacing the dimethyl phosphate with DI water were the cross-linked chitosan microspheres, labeled as CCM. The aluminum chelated cross-linked N-methylene phosphonic chitosan microspheres (Al-CPCM) were obtained by impregnation of saturated $Al_2(SO_4)_3$ solution from CPCM. The changes of molecular structure during the synthesis process of Al-CPCM resins are described in Fig. 2.

3. Characterization

The swelling of those microspheres was verified according to the method reported by Singh et al. [23]. About 0.1 g of the resins was weighed after being dried at 70 °C for 12 h, and the value was recorded as W_d. After that, the resins were swollen in DI water for 3 h following and then separated and blotted by filter paper to remove the surface water. At this time, the resin was weighed again and its weight was recorded as W_s. Thus, the swelling characteristics, equilibrium swelling ratio (E_{sr}) and equilibrium water content (E_{wc}) could be calculated through Eq. (1) and Eq. (2):

$$E_{sr} = \frac{W_s - W_d}{W_d} \quad (1)$$

$$E_{wc} = \frac{W_s - W_d}{W_s} \quad (2)$$

The size and surface morphology of the microspheres were observed by field-emission scanning electron microscopy (FE-SEM, Quanta 450, FEI, USA). And the surface elements were analyzed through the energy-dispersive X-ray (EDS) spectroscopy, an accessory of SEM. The crystalline information was analyzed by X-ray diffraction (XRD) using a X-ray diffractometer (X'Pert PRO, PANalytical, Netherlands) with Cu Kα radiation at 40 kV/40 mA, scan-

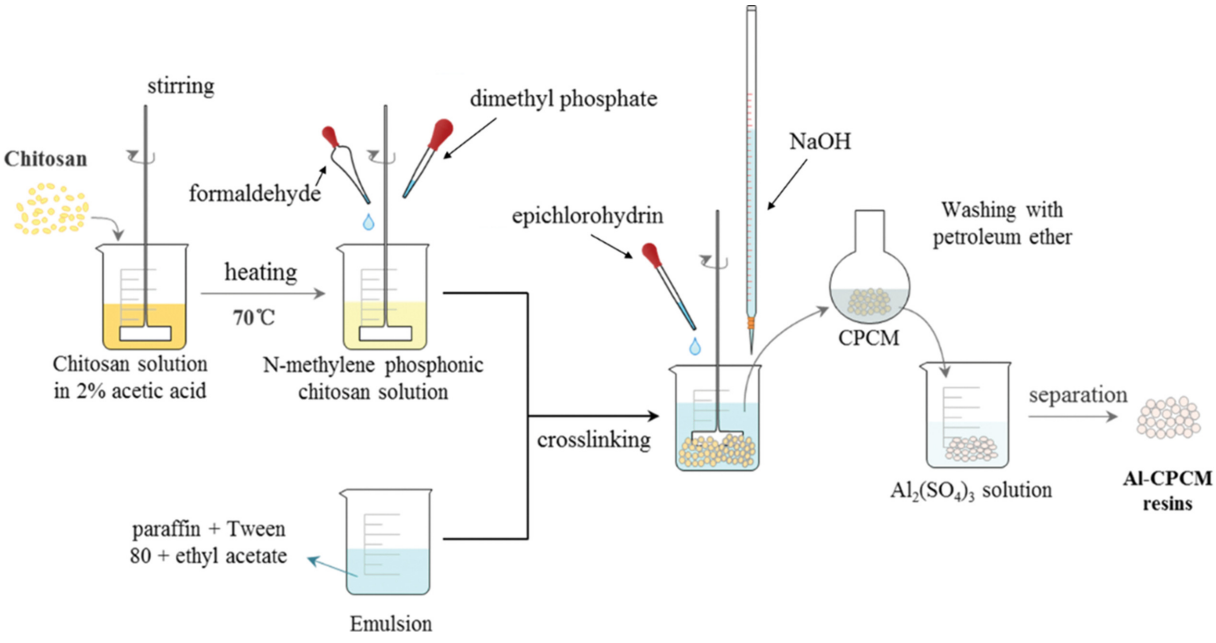

Fig. 1. The synthesis scheme of Al-CPCM resins.

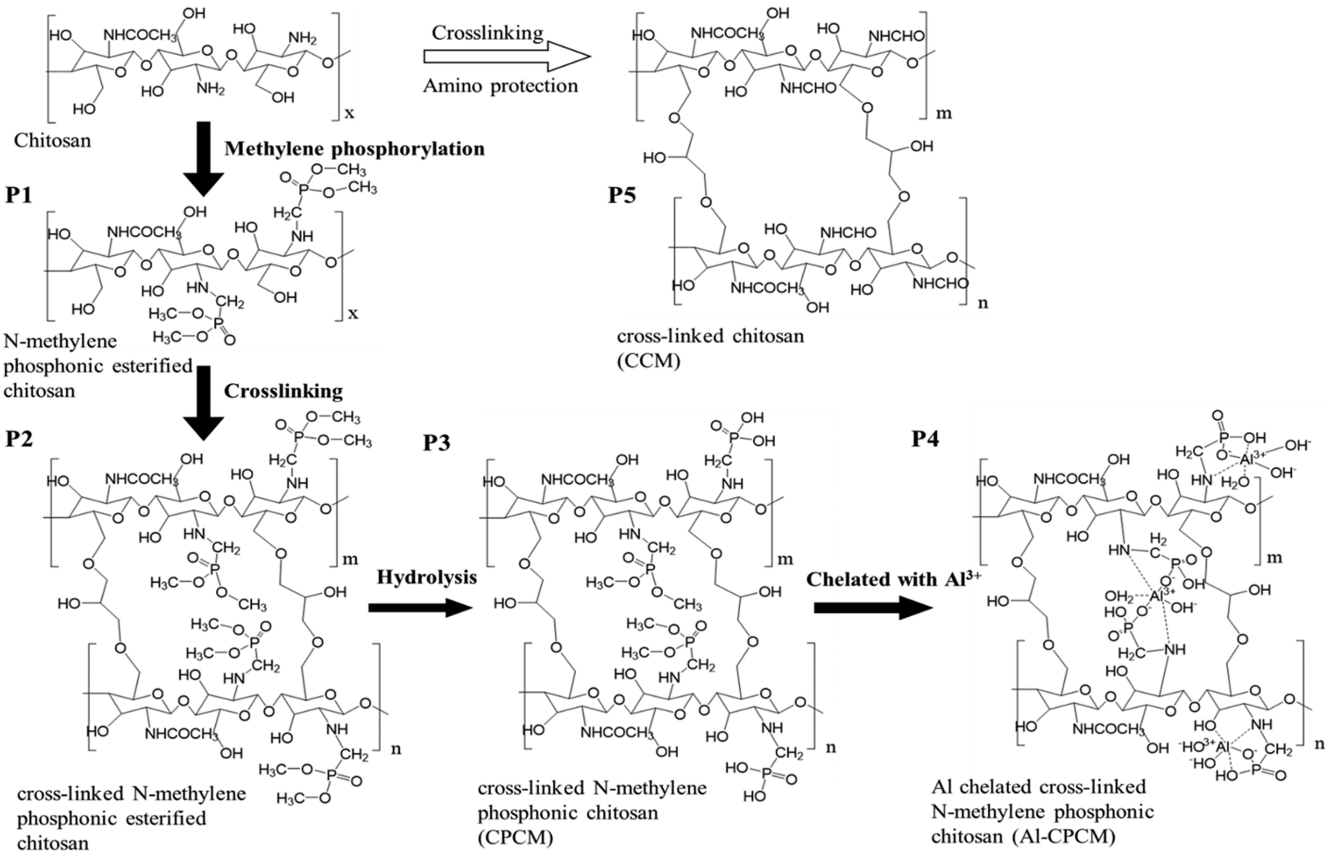

Fig. 2. The changes of molecular structure during the synthesis process of Al-CPCM resins.

ning angle 2θ from 10° to 80°. The BET surface area and pore structure were characterized by N_2 adsorption at −196 °C, supported by an automated gas ad-desorption system (AutosorbiQ-C, Quantachrome Instruments, USA). The thermostability was obtained by a thermogravimetric analyzer (SDTQ600, TA instruments, USA) with a heating rate of 10 °C/min under 100 mL/min nitrogen flow, from room temperature to 500 °C.

ATR-FTIR and *in situ* flow-cell ATR-FTIR spectroscopy (Nicolet iS50, Thermo Scientific, USA) were used to investigate the surface chemical composition and the change of complexation during adsorption. The *in situ* flow-cell ATR-FTIR was conducted in a single crystal germanium flow cell. A solution containing 2 mg/L of fluoride, which was adjusted to pH 7, was pumped through it by a chromatography pump, with the spectrum recorded every interval.

4. Batch Experiments

The batch adsorption experiments of F^- were conducted to investigate the effect on capacity, including initial pH, adsorbent dosage and co-existing anions, and obtain the process parameters of kinetics and thermodynamics to establish the mechanism. Typically, a certain volume of fluoride stock solution was added to a 50 mL centrifuge tube, and the stock solution was 500 mg-F/L prepared by the dissolution of sodium fluoride in DI water. After that, some granular adsorbents were weighted into it and then the tube was placed in a shaker with a temperature controlled incubator at 220 rpm for full contact. At every sampling time, 0.5 mL of solution was drawn with a syringe, filtered through a 0.22 μm filter and mixed with the same volume of ionic strength modifier so that the concentration could be recorded by fluoride selective electrode (Alpha, Thermo Scientific, USA). All experiments were performed in triplicate, and 0.04 M NaCl was added as background in all experiments except for that of co-existent anions.

4-1. Effect of pH, Adsorbent Dosage and Coexisting Anions

The effect of pH on the fluoride ion adsorption of resins was investigated in the range of pH 2 to 12. The experiments were carried out by adding 0.12 g of wet resins into a centrifuge tube containing 40 mL fluoride solution with the concentration of 20 mg/L, at 20 °C, for a contact time of 24 h. Before reaction, the initial pH of the solutions was adjusted by 0.01 or 0.1 M HCl or NaOH. However, the initial pH in experiment of adsorbent dosage was fixed at 7, but the weight of resins added varied from the solid-liquid ratio of 0.2 g/L to 10 g/L. After 24 hours, the residual fluorine concentration was recorded as well as the leaching aluminum, detected by ICP-OES (Optima 8000, PerkinElmer, USA).

The experiments of coexisting anions were performed by introducing the sodium salt of the corresponding anion. They were prepared to stock solutions of 2 g/L and injected into the reaction system before the adsorbent was added. The molar concentration of each coexisting ions was set to be equal, 5 times and 20 times to that of fluoride ions.

4-2. Kinetics

The adsorption kinetics was investigated in an Erlenmeyer flask containing 200 mL of fluoride solution. The concentration of fluo-

ride was 20 mg/L and the dosage of the wet resins was 0.6 g. The interval of time for sampling increased from 10 to 360 min. The kinetic results were analyzed by three common kinetic models: pseudo-first-order (PFO), pseudo-second order (PSO) and Elovich kinetic model. The three kinetic equations tried are those given below as integrated forms [24]:

$$Q_t = Q_e(1-e^{-k_1 t}) \quad (3)$$

$$Q_t = \frac{k_2 Q_e^2 t}{1+k_2 Q_e t} \quad (4)$$

$$Q_t = \frac{1}{\beta}\ln(\alpha\cdot\beta\cdot t) \quad (5)$$

where Q_t is the adsorption capacity of fluoride ions from initial to time t (mg/g); Q_e is the equilibrium adsorption capacity (mg/g); k_1 and k_2 are the rate constants of PFO (min^{-1}) and PSO (g/(mg·min)) kinetic model, respectively; α is the initial adsorption rate (mg/(g·min)) and β is the desorption constant (g/mg).

4-3. Isotherms and Thermodynamics Analysis

The equilibrium adsorption experiment was performed at fixed solid-liquid ratio of 3 g/L and initial pH of 7, while with variable initial concentration of F^- from 2.5 mg/L to 250 mg/L and different temperatures of 20 °C, 30 °C and 40 °C. Residual fluoride ions were detected after 24 h and the results were fitted to three isotherm models: Langmuir, Freundlich and Hill. The non-linear forms of them are shown in Eq. (6), Eq. (7) and Eq. (8), respectively:

$$q_e = \frac{q_m k_L C_e}{1+k_L C_e} \quad (6)$$

$$q_e = k_F C_e^{\frac{1}{n_F}} \quad (7)$$

$$q_e = \frac{q_m C_e^{n_H}}{K_H + C_e^{n_H}} \quad (8)$$

where the q_m is the maximum theoretical adsorption capacity on a monolayer surface (mg/g); k_L is Langmuir constant (L/mg), which reflects the energy of adsorption; k_F is Freundlich constant, related to the amount of the fluoride ions on per gram of beads at the equilibrium concentration ($mg^{1-1/n}\cdot L^{1/n}\cdot g^{-1}$); n refers to the strength of the adsorption process and the distribution of active sites on the surface heterogeneity; k_H is the Hill constant (mg/L), and n_H is the Hill cooperativity coefficient, which is a sign that reflects whether there is mutual influence between active sites, if n_H=1, there is no mutual interference, if n_H>1, positive cooperativity, and negative cooperativity when n_H<1 [25].

The thermodynamics analysis was applied based on the data of isotherms. In the equilibrium process, Gibbs free energy ΔG^o (J/mol) could be calculated in each concentration as shown in Eq. (9):

$$\Delta G^o = -RT\ln\left(\frac{\rho q_e}{C_e}\right) \quad (9)$$

where R is the universal gas constant (8.314 J/mol·K^{-1}); T is the temperature (K); ρ is the dried density of adsorbent; and q_e and C_e are the same as in the isotherm.

The enthalpy change (ΔH^o, J/mol) and entropy change (ΔS^o, J/mol·K^{-1}) in adsorption could be regressed by van't Hoff equation (Eq. (10)):

$$R\ln\left(\frac{\rho q_e}{C_e}\right) = \Delta S^o - \frac{\Delta H^o}{T} \quad (10)$$

4-4. Desorption and Reusability

Reusability of the Al-CPCM resins was evaluated by six rounds of adsorption/desorption cycles. The condition of the adsorption experiment was the same as that of the kinetic experiment. Each round of adsorption lasted for 24 h followed by desorption after the fluorine adsorption capacity was recorded. For desorption experiment, the used 2 g of beads were separated and soaked in 20 ml of 100 g/L $Al_2(SO_4)_3$ solution for 6 h, and then washed with DI water until the eluate was neutral for tge next round. Before this, the concentration of AlF_6^{3-} in the $Al_2(SO_4)_3$ solution was measured by the electrode and recorded [26].

5. Column Experiments

The column experiments were performed in a φ16×100 mm class tube with an inner diameter of approximately 12 mm. A volume of 10 mL of Al-CPCM resins was filled into it. The height of the resin bed was 89 mm with an approximate voidage of 0.46. The groundwater sample was pumped to flow through the column at different empty bed contact times (EBCTs) of 2.5 min (24 BV/h), 5 min (12 BV/h) and 10 min (6 BV/h). The groundwater sample was taken from a tube well in Yingjing County, Sichuan Province, PRC, and its detailed parameters are presented in Table S1. The pH of the effluent and the concentration of F^- and Al^{3+} in it were monitored during the whole process.

The regeneration of the column was completed by pumping 30 mL of high-concentration aluminum sulfate solution (100 g/L of $Al_2(SO_4)_3\cdot 18H_2O$) cyclically for 3 h with a flow a rate of 30 BV/h at room temperature. The AlF_6^{3-} in the elution was detected every 10 min. Then 60 mL of fluorine-free water was pumped to wash for next adsorption.

The breakthrough data of column experiments were fitted by the Dose-Response model. This is an empirical model without any assumptions about fundamental uptake behavior and can provide the best description of fluoride breakthrough, as shown in Eqs. (11) and (12):

$$\frac{C}{C_{in}} = 1 - \frac{1}{1+\left(\frac{v_{ef}}{b}\right)^a} \quad (11)$$

$$q_0 = \frac{bC_{in}}{m} \quad (12)$$

where C is the current concentration of effluent (mg/L); C_{in} is the concentration of inlet solution (mg/L); v_{ef} is the volume of solution discharged out of the column (L); a and b are model constants; q_0 is the theoretical dynamic maximum adsorption capacity of resin (mg/g); and the m is the dry mass of resin (g).

RESULTS AND DISCUSSION

1. Synthesis and Characterization of the Al-CPCM Resins

1-1. Synthesis

As shown in Fig. 2, when formaldehyde and dimethyl phosphate

were added to the chitosan solution, the amino groups on chitosan formed Schiff bases-NHCHO with formaldehyde [22,27], which thus provided a dehydration grafting site for dimethyl phosphate, generating N-methylene phosphonic esterified chitosan (P1) [28]. In the structure of this intermediate, except for the hydroxyl groups on chitosan, there were no other sites that reacted with the cross-linking agent, epichlorohydrin [29]. Therefore, the P2 was obtained through the cross-linking reaction in the emulsion. As the alkalinity of the mixture increased, cross-linked polymers became hardened and the phosphonic esters hydrolyzed to P3 [30]. This obtained product was cross-linked N-methylene phosphonic chitosan microspheres (CPCM). And it has ability to chelate polyvalent metal like other amino-methyl phosphonic resins. Thus, the Al-CPCM resins (P5) were obtained by complexing CPCM with Al^{3+}.

The whole synthesis process would was further illustrated based on followed characterizations. For comparison, cross-linked chitosan (CCM, P5) was also synthesized, and formaldehyde was also needed to avoid the reaction between amino group and epichlorohydrin [31], to obtain the same polymer structure as CPCM.

1-2. Swelling Characteristics

The equilibrium swelling ratio and equilibrium water content of CCM, CPCM and Al-CPCM calculated from Eq. (1) and Eq. (2) are given in Table 1. It was shown that these polymer microspheres all showed good swelling characteristics with high water content. The E_{sr} and E_{wc} values of CPCM sample increased considerably compared with CCM, but they both dropped significantly after being complexed with Al^{3+}. This was related to the change in hydrophilicity caused by the introduction and conversion of phosphonic groups [32,33].

Table 1. The swelling behavior of CCM, CPCM and Al-CPCM

Resin	Equilibrium swelling ratio (%)	Equilibrium water content (%)
CCM	42.85	30.28
CPCM	257.4	72.33
Al-CPCM	20.51	17.21

1-3. Morphology and BET Analysis

The SEM image of pre- and post-adsorbed Al-CPCM microspheres is shown in Fig. 3(a) and (b). It is shown that the polymer beads synthesized in the emulsion are a regular spherical shape with all particle sizes less than 1 mm. For a more micro scale below 1 μm, the rough surface of the resin with rich pore structure can be observed. And no obvious difference was found in morphology of the two microspheres samples before and after adsorption. Besides, the EDS analysis results of them are given in Fig. 3(c) and (d), respectively. The weight percentage of 8.21% of aluminum in pre-adsorbed sample revealed its effective complexation with CPCM, which was close to the value of 8.29% calculated from TGA curves of Al-CPCM and CPCM (Fig. S1). Besides, the significant appearance of fluorine content in post-adsorbed sample donated the successful fluoride adsorption by Al-CPCM.

Fig. S2 shows the results of BET N_2 adsorption-desorption characterization for CPCM and Al-CPCM. The adsorption-desorption curves of both two samples presented type IV isotherm with an H2 hysteresis loop, which suggests the disordered pore structure and the various pore types [34,35], including macro-, meso-,

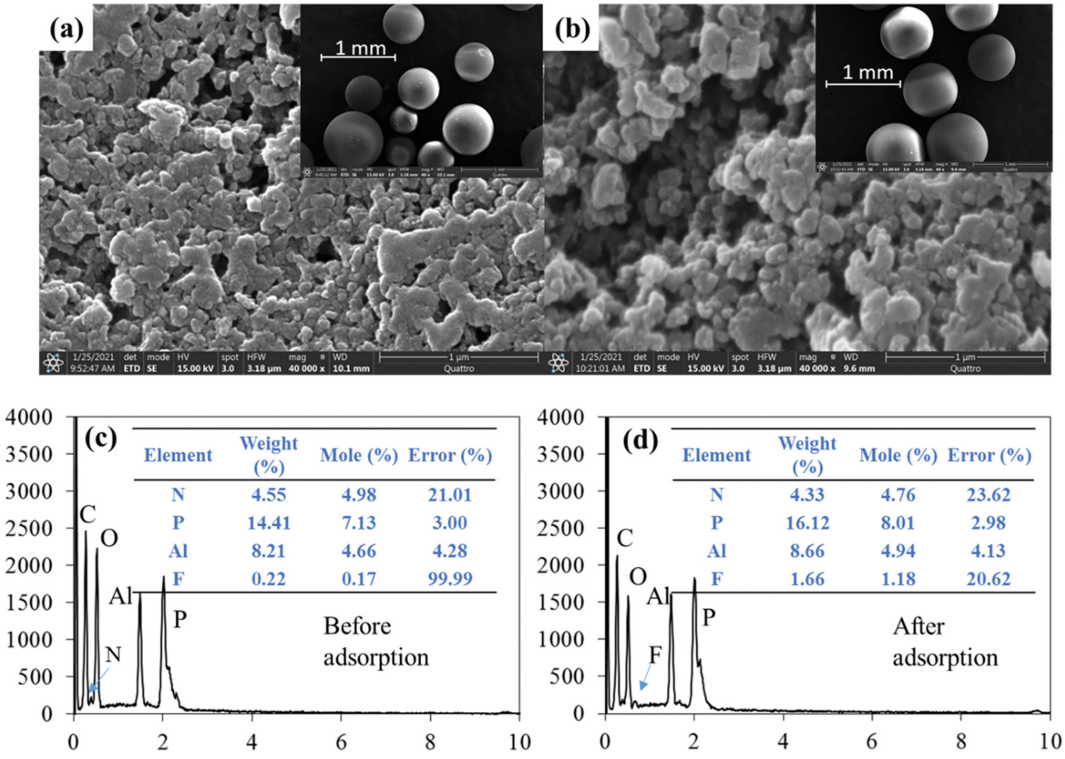

Fig. 3. The SEM images and EDS analyzation of pre- and post-adsorbed Al-CPCM.

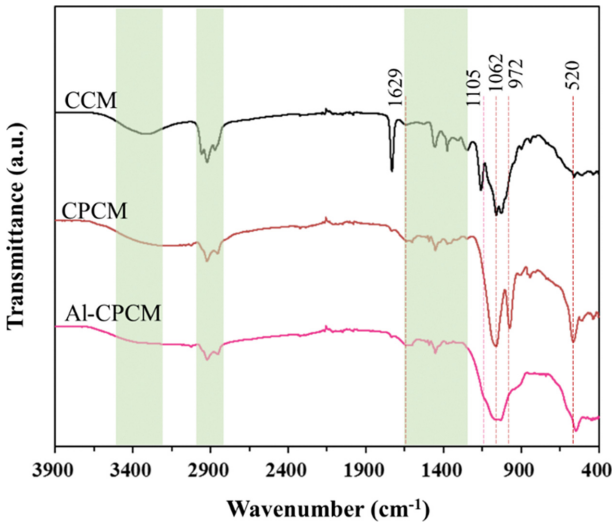

Fig. 4. The FTIR spectra of CCM, CPCM and Al-CPCM.

and micropores. The BET specific surface area (S_{BET}), pore volume and average pore diameter of CPCM resin was 15.07 m^2/g, 0.23 cm^3/g and 58.67 nm, respectively. However, compared with CPCM, Al-CPCM had a larger S_{BET} of 36.74 m^2/g but a smaller pore volume and size decrease of 0.18 cm^3/g and 19.39 nm, respectively. This might be attributed to the complexation of Al^{3+} between adjacent chitosan molecules in the network structure [36,37], as P4 in Fig. 2.

1-4. Spectroscopy Analysis

The FTIR spectra in Fig. 4 illustrate the transmutation of the functional groups in synthesis of Al-CPCM. It is obvious that the CPCM obtained by cross-linking after phosphorylation some identical major bands remained with the CCM. The attribution of these common peaks is listed in Table S2. Compared with the spectrum of CCM, the peak of -CHO at 1,715 cm^{-1} was not found in the spectrum of CPCM, which was attributed to the methylene phosphorylation. Meanwhile, the formation of -NH-CH_2- also obstructed the vibration of N-H, leading to a weaker response peak, and gave a slight enhancement to the peak of C-N bending vibration at 1,629 cm^{-1} [33,38]. The stretching vibration peaks of C-O in the spectrum of CPCM were overlapped by two new ones present at 1,062 and 972 cm^{-1}. The former was the stretching vibration peaks of P-O and the latter was attributed to the triply degenerated asymmetric stretching of phosphonic group. The bending vibration peak of P-O emerged at 520 cm^{-1} [39,40]. These above might demonstrate the successful N-methylene phosphorylation.

In the spectrum of Al-CPCM, the intensity of peak at 972 cm^{-1} became weaker, compared with that of CPCM. The inhibition of asymmetric stretching of phosphonic group indirectly suggests the formation of P-O-Al. And the new shoulder peak emerged at 1,105 cm^{-1} might be ascribed to the stretching of Al-O of the surface hydroxyl of complexed Al^{3+} [41,42]. In addition, the vibration peak of O-H and N-H in hydroxyl and imino groups of chitosan became further weaker and broader, which might indicate the coordination between Al^{3+} and them.

The XRD patterns are shown in Fig. S3. The diffraction patterns of all three samples confirm an overall amorphous characteristic of chitosan. The broadband around 20° and the shoulder band at 12° indicates the low crystalline Form I and Form II by intramolecular hydrogen bond [43]. The decrease of the intensity of shoulder band suggests that the both methylene phosphonate and Al^{3+} complexation might reduce crystallinity. In the XRD pattern of Al-CPCM, the broadband around 20° occurs, an obvious shifting towards large 2θ angle, and this might be attributed to the chelation of Al^{3+} between adjacent molecular of chitosan, which could increase the layer spacing of the polymer [44,45].

2. The Batch Adsorption Performance

2-1. Effect of Adsorbent Dosage and Initial pH

Fig. 5(a) shows changes of fluoride adsorption as a function of the concentration of Al-CPCM. It is shown that the removal efficiency of F^- increased with the addition of resins, ascribed to more active sites available for adsorption. Further, it no longer increased significantly at the dosage up to 0.3 g/L. Hence, the solid-liquid ratio of 0.3 g/L was selected for the subsequent adsorption ratio.

To explore the influence of the initial pH on the adsorption of fluoride, the pH edge experiment was carried out and the results are given in Fig. 5(b). It is obvious that the initial pH affected the fluoride ion adsorption on Al-CPCM beads. The F^- removal efficiency stayed higher than 85% on average from pH 3 to pH 10. And the leaching of aluminum was also able to be maintained below 30 μg/L. There was a little improvement of the removal capac-

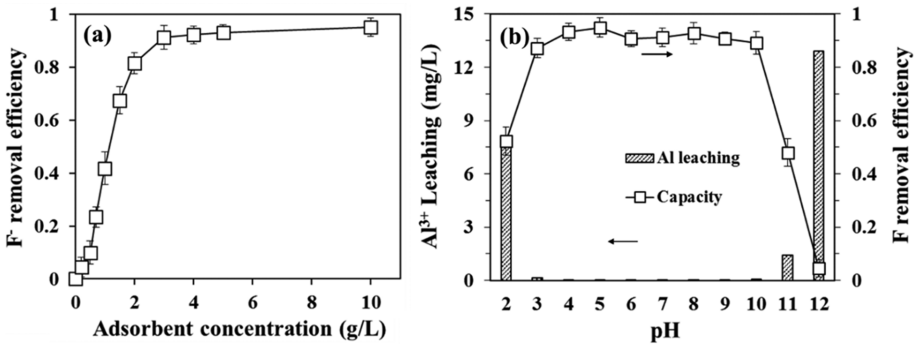

Fig. 5. The results of effects of (a) adsorbent dosage; and (b) initial pH on fluoride adsorption (Experimental conditions: adsorbent dosage: 3 g-wet beads/L; initial pH 7; initial concentration of F^-: 20 mg/L; temperature: 20 °C; shaking speed: 220 rpm; contact time: 24 h; background: 0.04 M NaCl).

ity at pH 4 and 5, probably related to the protonation of imino in Al-CPCM [46]. However, no matter when the pH was beyond 10 or below 3, the adsorbed fluoride ion content decreased significantly. This was largely because of the decomplexation of Al^{3+} due to the amphoterism of aluminum [9,47], which made F^- lose its binding site, with almost no adsorption capacity of CPCM for fluorine (shown in Fig. S4). The decomplexation could also be confirmed by the massive Al^{3+} leaching at pH 2, 11 and 12. Nevertheless, Al-CPCM still performed a wide adaptation for effective F^- adsorption.

2-2. Adsorption Kinetics

The kinetic data of the adsorption of fluoride ions on Al-CPCM resins fitted by the PFO, PSO and Elovich models are presented in Fig. 6. As can be seen, fluoride adsorption onto Al-CPCM took place rapidly in the first 40 min, attributed to excess binding sites of chelated Al^{3+} [11]. Compared with the PFO and Elovich PFO kinetic models, the PSO kinetic model had the highest fitting degree with an R^2 of 0.998, and the calculated value of Q_e was more consistent with the experimental one. It indicated that the PSO kinetic model could better describe the adsorption process of F^- on Al-CPCM, which might assume the chemical adsorption of electron-sharing or transfer between the adsorbate and adsorbent. Therefore, the removal of fluoride by the resins might be dominated by a coordination interaction like surface complexation [10,48]. R^2 of the PSO kinetic model was above 0.98, suggesting that intraparticle diffusion was also not negligible. And the experimental data obtained did not fit well the Elovich kinetic model, indicating the insignificant change of activation energy in the adsorption of F^- [49].

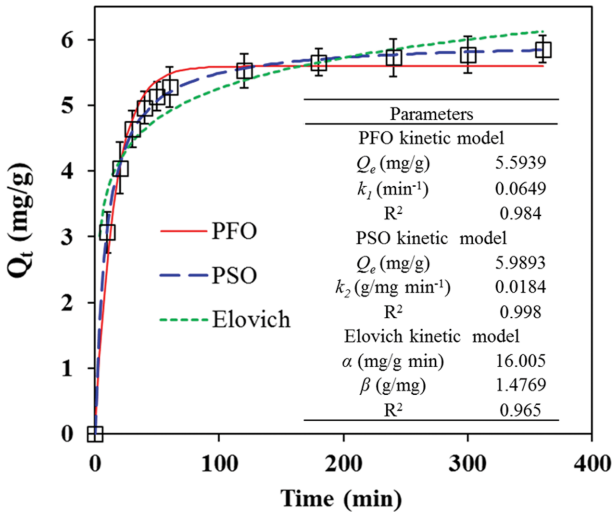

Fig. 6. The adsorption kinetic fitting curves and parameters of fluoride on Al-CPCM resins (Experimental conditions: adsorbent dosage: 3 g-wet beads/L; initial concentration of F^-: 20 mg/L; initial pH 7; temperature: 20 °C; shaking speed: 220 rpm; background: 0.04 M NaCl).

2-3. Isotherms and Thermodynamics Analysis

Fig. 7(a)-(c) illustrate the fitting results of experimental data by Langmuir, Freundlich and Hill isotherm models at various temperatures, and the relevant parameters are shown in Table 2. It is obvious that the fitting results of the Langmuir and its improved

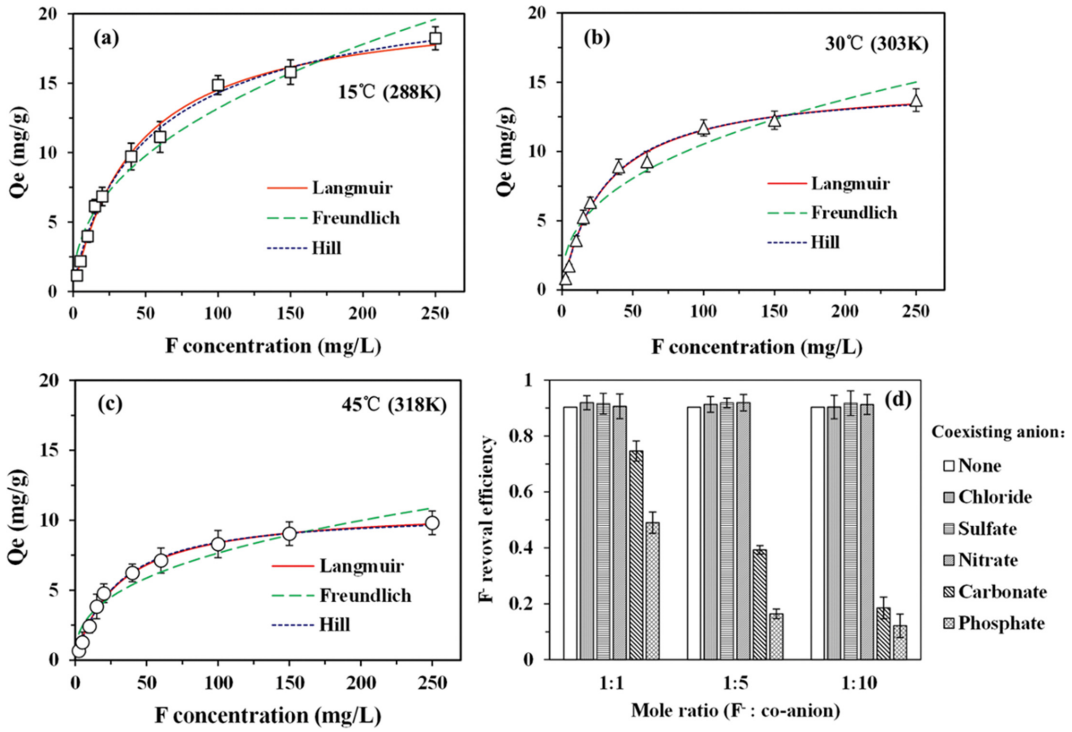

Fig. 7. The adsorption isotherms at 15 °C (a), 30 °C (b) and 45 °C (c), and effect of coexisting anions of fluoride on Al-CPCM resins (d) (Experimental conditions: adsorbent dosage: 3 g-wet beads/L; initial pH 7; shaking speed: 220 rpm; contact time: 24 h; background: 0.04 M NaCl for isotherm).

Table 2. The fitting parameters of isotherms

	288 K	303 K	318 K
Langmuir model			
q_m (mg/g)	20.841±0.663	15.067±0.414	10.891±0.242
k_L (L/mg)	0.026±0.002	0.033±0.003	0.034±0.002
R^2	0.993	0.992	0.994
Freundlich model			
k_F ($mg^{1-1/n}\cdot L^{1/n}\cdot g^{-1}$)	1.799±0.316	1.775±0.378	1.314±0.284
1/n	2.312±0.198	2.586±0.307	2.614±0.318
R^2	0.965	0.926	0.921
Hill model			
k_H (mg/L)	33.649±1.931	32.353±7.621	34.059±6.584
q_m (mg/g)	23.158±5.314	14.862±0.831	10.578±0.433
n_F	1.153±0.103	0.947±0.096	0.942±0.073
R^2	0.995	0.991	0.995

Table 3. The thermodynamics data of fluoride adsorption on Al-CPCM

F concentration (mg/L)	ΔH^o (kJ/mol)	ΔS^o (J/mol·K^{-1})	ΔG^o (kJ/mol)		
			293 K	303 K	313 K
2.5	−13.55	93.5	−13.4654	−14.6442	−16.2712
5	−13.46	93.2	−13.3418	−14.8023	−16.1364
10	−12.52	89.7	−13.1997	−14.8736	−15.8901
15	−11.86	87.7	−13.3318	−14.8071	−15.9614
20	−9.04	77.4	−13.1698	−14.5593	−15.4917
40	−11.13	81.2	−12.1483	−13.6727	−14.5846
60	−11.32	79.3	−11.4934	−12.7540	−13.8725
100	−14.76	88.3	−10.6374	−12.0563	−13.2865
150	−14.16	83.5	−9.8710	−11.1506	−12.3755
250	−15.69	85.2	−8.8461	−10.1456	−11.4031

form Hill model suitable to describe the adsorption process of F^-, due to the high values of R^2, located in the range of 0.991 to 0.995 at all three temperatures. The Langmuir maximum adsorption capacity of 15.067 mg/g at 30 °C was satisfactory. And it might assumed that the adsorbate combined onto specific homogeneous sites of the adsorbent with a monolayer coverage, rather than the electrostatic multi-layer adsorption confirmed from Freundlich isotherm model. In addition, the n_H value of Hill model at each temperature was near to 1, signifying that there was almost no competition between fluoride and chloride in the background. This was verified in the co-existing anion experiment [50,51].

The regression data of thermodynamics analysis is listed in Table 3. The negative values of ΔG^o, the negative values of ΔH^o and the positive values of ΔH^o suggest that the adsorption process is spontaneous, exothermic and has increased entropy. The ΔG^o value decrease with the increase in temperature confirmed that a relatively low temperature was favorable to the adsorption of F^- on Al-CPCM. The value of $|\Delta H^o|$ reduced with the adsorbate increase, indicating that the physical adsorption would become more dominant with the equilibrium concentration of fluorine. And the values of ΔS^o revealed the increase of the randomness at the solid/liquid interface and the interaction between F^- and the active sites of Al-CPCM resins [52,53].

2-4. Effect of Coexisting Anions

The effect of coexisting anions on the removal efficiency of fluoride is shown in Fig. 7(d). As can be seen, the existence of chloride, sulfate and nitrate presents almost no negative effect on the removal efficiency of fluoride, even when the concentrations of them are much higher than that of fluorine. However, the presence of both carbonate and phosphate could bring a considerable decrease in the removal efficiency of F^-, and the inhibitory becomes more severe with the increase of their concentration. Because the solution had been adjusted to pH 7 after adding the co-anions, this negative effect should not be attributed to alkalinity but might be competitive adsorption. Fluoride ions may directly form inner complexes with chelated aluminum in Al-CPCM, so that it was not interfered by the common anions like chloride, adsorbed on the outer spheres [9,54].

2-5. Desorption and Reusability

The result of successive sorption/desorption cycles of fluoride on Al-CPCM is presented in Fig. S5. Having in mind that the decomplexation of Al^{3+} occurred under investigation in this work at a high acidity or alkalinity, it was presumed that the desorption and regeneration could be achieved by aluminum sulfate solution

with high-concentration, like some commercial defluorinated resins did [55]. As can be seen in Fig. S5, the adsorption capacity of the next round is basically equal to the desorption capacity of the previous round. The adsorption capacity of F^- decreased with 4.32% to 5.75 mg/g in the second round, compared with the 6.01 mg/g of the first round, which might be attributed to the few irreversible complexation sites [56]. Nevertheless, no appreciable loss in the adsorption capacity was found during the next five rounds of consecutive sorption/desorption cycles, with a stable fluorine adsorption capacity of about 5.68 mg/g. These results show that the Al-CPCM resin could be almost completely regenerated and repeatedly used.

3. Adsorption Mechanism

The proposed adsorption mechanism of fluoride on the Al-CPCM resins is shown in Fig. 8. According to the results of several characterizations, kinetics, isotherms and thermodynamics, the ion exchange process based on chemisorption was more convincing [10,36,57]. As can be seen in Fig. 8, except for the slight electrostatic attraction of protonated imino group under slightly acidic conditions, the dominant binding sites of fluoride ion were the chelated Al^{3+} in various forms. In particular, the F^- would replace the surface hydroxyl of the chelated Al^{3+} in Al-CPCM, which was confirmed by the emerging Al-F bond in Al 2p XPS spectra of post-adsorption resin and the negative absorbance of the v(Al-OH) peak at 1,105 cm^{-1} in *in-situ* FTIR spectra (Fig. S6). Moreover, this process was mainly affected by pH. As shown in Fig. S6, there was another negative peak in the *in-situ* FTIR spectra at pH 3 and pH 11, respectively. This suggests the decrease of P-O-Al and reveals

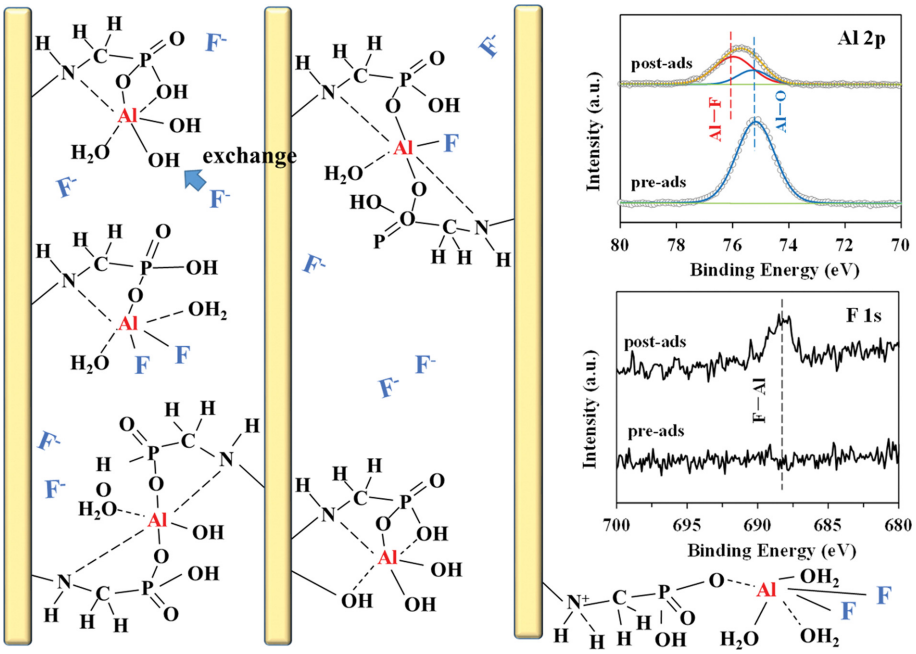

Fig. 8. The proposed adsorption processes of fluoride on Al-CPCM resins.

Table 4. The fluoride adsorption capacity comparisons of different resins

Adsorbents	Resin dosage (g/L)	Concentration of F^- (mg/L)	Adsorption capacity (mg/g)	Desorption	Cycle times	Decrease of adsorption capacity	Ref.
Zr^{4+} incorporated chitosan resin	2	20	4.33	0.05 M NaOH	5	26.1%	[45]
Al^{3+} chelated Monoplus TP 260	15	25	6.11	123.49 g/L $Al_2(SO_4)_3$	3	17.6%	[11]
La^{3+} chelated MTS9501 resin	10	500	5.07	0.01 M NaOH	5	15.1%	[57]
Purolite A520E resin	2	5	1.85	6% NaCl at 50 °C	3	2.4%	[58]
Al^{3+} chelated Indion FR10 resin	50	3	0.478	0.1 M HCl+10% $Al_2(SO_4)_3$	3	10%	[59]
Al-CPCM resin	3	20	5.68	100 g/L $Al_2(SO_4)_3$	6	5.5%	This study

*The comparison is based on data collected on pure, synthetic NaF solutions

the dissociation of chelated aluminum, which is consistent with the result of Section 3.2.1.

4. Fluoride Adsorption Capacity Comparisons Among Different Adsorbents

Aiming for a better investigation, the fluoride adsorption performance comparisons among various fluorine selective resin are concluded in Table 4. Practically, as the polyvalent metal-incorporated resin, the Al-CPCM demonstrates a satisfactory capacity of 5.68 mg/g and an advantage of stable regeneration. The remarkable performance is at least not inferior to other chelating resins modified by Al(III), Zr(IV) and La(III).

5. Column Experiments

The results of column adsorption of fluoride from actual groundwater by Al-CPCM resin are shown in Fig. 9, including breakthrough curves of two rounds of dynamic adsorption at three different flow rates in Fig. 9(a)-(c) and their elution profiles in Fig. 9(d). The breakthrough curves are well described by Dose-Response model with the fitting data listed in Table S3, and some adsorption/desorption capacities are summarized in Table 5. Here, the breakthrough point was set at a concentration of F^- lower than 1.5 mg/L, which was the limit value of fluoride in drinking water from WHO [60]. The breakthrough point at rates of 6 BV/h, 12 BV/h and 24 BV/h in first round are 800 BV, 480 BV and 350 BV, respectively. The accumulated fluoride adsorption capacity was 1.55 mg/g, 0.93 mg/g and 0.64 mg/g. All of them decreased with the increase of flow because of the insufficient contact at fast feeding. It is worth noting that the accumulated fluoride adsorption capacity was much lower than the capacity obtained in static adsorption. In addition to the restricted mass transfer in the column, the large amount of phosphate and carbonate in groundwater might be the main reason for this decrease [57,61].

The elution was performed before the second adsorption. As seen in Fig. 9(d), the fluoride concentration in the eluate of 6 BV/h, 12 BV/h and 24 BV/h feeding rates all increased rapidly and stabilized at 467 mg/L, 295 mg/L and 207 mg/L, respectively, within 80 min. The calculated desorption capacities were 1.402 mg/g, 0.889

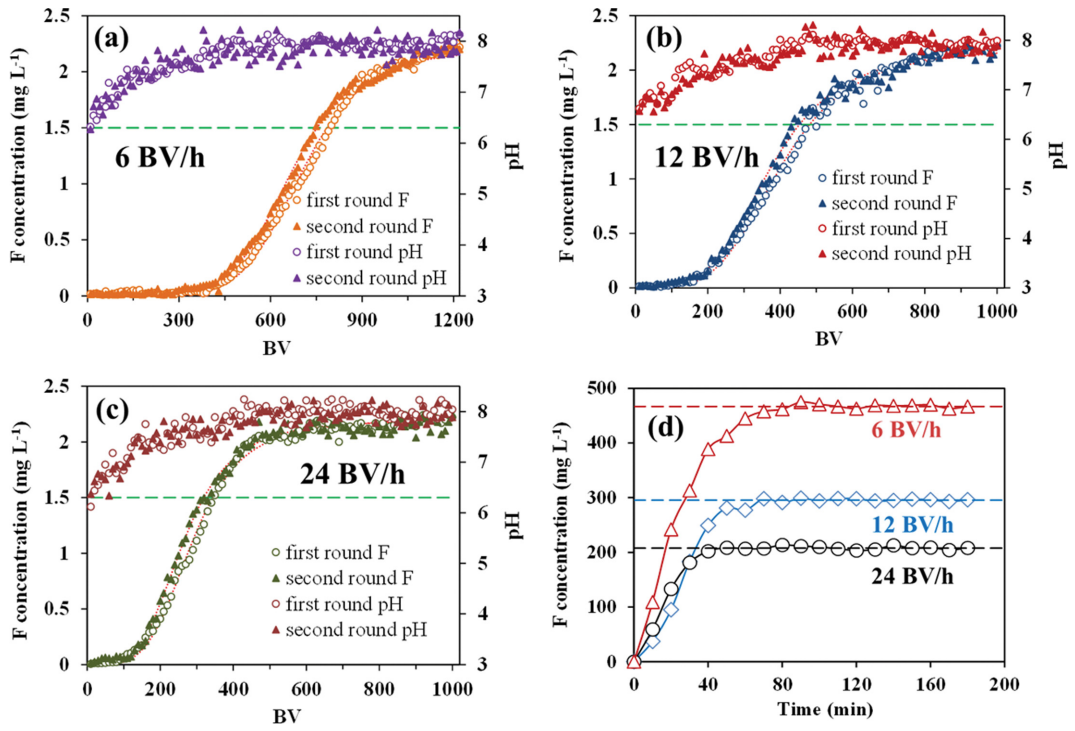

Fig. 9. The (a) breakthrough curves of the column experiment for fluoride adsorption on Al-CPCM resins at flow rate of (a) 6 BV/h, (b) 12 BV/h and (c) 24 BV/h; (d) elution curves of the column experiment for three different feeding flow rates (Experimental conditions: column volume: 10 mL, Φ=10 mm; elution: 100 g/L of $Al_2(SO_4)_3 \cdot 18H_2O$; elution method: circulate for 3 hours at 30 BV/h).

Table 5. The column data for fluoride removal from groundwater by Al-CPCM resins

Flow rate (BV/h)	6		12		24	
	Round 1	Round 2	Round 1	Round 2	Round 1	Round 2
Break point (BV)	800	750	480	450	350	340
Breakthrough capacity (mg/g wet resin)	1.471	1.342	0.824	0.763	0.591	0.553
Total capacity (mg/g wet resin)	1.554	1.389	0.934	0.882	0.645	0.616
Total desorption capacity (mg/g wet resin)	1.402	-	0.887	-	0.623	-
Total elution efficiency	90.22%	-	94.96%	-	96.61%	-

mg/g and 0.623 mg/g with the elution efficiency was 90.22%, 94.96% and 96.61%, respectively. It could be found that slower flow rate had a negative effect on the elution efficiency. This might be caused by more irreversible sites being occupied at low flow rate. In the second round, the breakthrough point decreased to 750 BV, 450 BV and 340 BV, respectively, and the total adsorption capacity of each flow rate was 1.389 mg/g, 0.882 mg/g and 0.616 mg/g, which was almost equal to the desorption capacity in elution.

Aluminum in effluent was analyzed five times at 10, 100, 400, 700 and 1,000 BV during adsorption in both two rounds of each feeding rate. The concentrations were always below 50 μg/L, indicating the chemical stability of Al-CPCM in actual groundwater.

CONCLUSION

Al(III) incorporated cross-linked N-methylene phosphonic chitosan microspheres (Al-CPCM) were obtained by cross-linking chitosan with epichlorohydrin from an improved emulsion method. As a defluorinated resin, its adsorption performance for aqueous fluoride was thoroughly investigated. It exhibited high adsorption capacity from pH 3 to 10, fast adsorption rate, favorable selectivity relative to Cl^-, SO_4^{2-} and NO_3^- in batch experiments employing pure, synthetic sodium fluoride solutions. The result of XPS, FTIR as well as the isotherms and thermodynamics studies supported that the chelated Al^{3+} was the dominant binding site of fluoride. F^- adsorption onto it through ion exchange with surface hydroxyl was spontaneous and exothermic. Also, the result of sorption/desorption experiment (handling synthetic NaF solution) revealed better regeneration efficiency of Al-CPCM among other defluorinated resins. Column experiment with a ground water sample indicated lower adsorption efficiency of the resin and larger decrease in adsorption efficiency after elution. This must be attributed to the presence of alternate anions and cations in ground water. More elaborate studies with ground water in adsorption columns are required to establish the commercial acceptance of the proposed resin/adsorbent.

CONFLICTS OF INTEREST

There are no conflicts to declare.

ACKNOWLEDGEMENTS

This study was supported by the Natural Science Foundation of China (grant numbers 51508564) and the Natural Science Foundation of Chongqing (grant numbers cstc2020jcyj-msxmX0405).

SUPPORTING INFORMATION

Additional information as noted in the text. This information is available via the Internet at http://www.springer.com/chemistry/journal/11814.

REFERENCES

1. S. Srivastava and S. Flora, *Curr. Environ. Health Rep.*, **7**, 140 (2020).
2. D. Huang, J. Yang, X. Wei, J. Qin, S. Ou, Z. Zhang and Y. Zou, *Environ. Pollut.*, **222**, 118 (2017).
3. X. He, P. Li, Y. Ji, Y. Wang, Z. Su and V. Elumalai, *Expo. Health*, **12**, 355 (2020).
4. P. Sharma, J. Baruah, D. Deka and P. Kaushik, *Harnessing wetlands for sustainable livelihood*, Notion Press, Chennai (2019).
5. J. Chen, H. Wu, H. Qian and Y. Gao, *Expo. Health*, **9**, 183 (2017).
6. C. Wu, X. Wu, C. Qian and G. Zhu, *Appl. Geochem.*, **98**, 404 (2018).
7. S. Meenakshi and N. Viswanathan, *J. Colloid Interface Sci.*, **308**, 438 (2007).
8. D. H. Phillips, B. S. Gupta, S. Mukhopadhyay and A. K. S. Gupta, *J. Environ. Manage.*, **215**, 132 (2018).
9. G. J. Millar, S. J. Couperthwaite, D. B. Wellner, D. C. Macfarlane and S. A. Dalzell, *J. Water. Process Eng.*, **20**, 113 (2017).
10. R. Li, X. Tian, I. Ashraf and B. Chen, *J. Chromatogr. A*, **1613**, 460697 (2020).
11. E. Shin, D. Dreisinger and A. Burns, *Desalination*, **505**, 114985 (2021).
12. J. Ding, L. Pu, Y. Wang, B. Wu, A. Yu, X. Zhang, B. Pan, Q. Zhang and G. Gao, *Environ. Sci. Technol.*, **52**, 12602 (2018).
13. S. Jana, J. Ray, B. Mondal, S. Pradhan and T. Tripathy, *Colloids Surf. A Physicochem. Eng. Asp.*, **553**, 472 (2018).
14. M. Zhang, P. Yang, G. Lan, Y. Liu, Q. Cai and J. Xi, *Environ. Sci. Pollut. R.*, **27**, 38617 (2020).
15. R. Liu, J. Du, Z. Zhang, H. Li, J. Lu, Y. Cheng, Y. Lv and H. Wang, *Carbohydr. Polym.*, **205**, 83 (2019).
16. B. G. Kwon, S.-Y. Chung, S.-S. Park and K. Saido, *Environ. Pollut.*, **234**, 167 (2018).
17. L. N.Pincus, P. V. Petrović, I. S. Gonzalez, E. Stavitski, Z. S. Fishman, H. E. Rudel, P. T. Anastas and J. B. Zimmerman, *Chem. Eng. J.*, **412**, 128582 (2021).
18. L. N. Pincus, F. Melnikov, J. S. Yamani and J. B. Zimmerman, *J. Hazard. Mater.*, **358**, 145 (2018).
19. Q. Liu, L. Zhang, B. Yang and R. Huang, *Int. J. Biol. Macromol.*, **77**, 15 (2015).
20. L. Jinfang, L. Qian, R. Huang and W. Guodong, *J. Rare. Earth.*, **34**, 1053 (2016).
21. R. Karthik and S. Meenakshi, *Int. J. Biol. Macromol.*, **67**, 210 (2014).
22. R. Antony, T. Arun and S. T. D. Manickam, *Int. J. Biol. Macromol.*, **129**, 615 (2019).
23. T. Singh, P. A. Mccarron, A. D. Woolfson and R. F. Donnelly, *Eur. Polym. J.*, **45**, 1239 (2009).
24. R. S. Juang and M. L. Chen, *Ind. Eng. Chem. Res.*, **36**, 813 (1997).
25. A. V. Hill, *J. Physiol.*, **40**, 190 (1910).
26. P. Palimaka and S. Pietrzyk, *Arch. Metall. Mater.*, **59**, 71 (2014).
27. Z. Guo, R. Xing, S. Liu, Z. Zhong, X. Ji, L. Wang and P. Li, *Carbohyd. Res.*, **342**, 1329 (2007).
28. V. Ramos, N. Rodrıguez, M. Dıaz, M. Rodrıguez, A. Heras and E. Agullo, *Carbohydr. Polym.*, **52**, 39 (2003).
29. C.-Y. Chen, C.-Y. Yang and A.-H. Chen, *J. Environ. Manage.*, **92**, 796 (2011).
30. C. Bunton, M. Mhala, K. Oldham and C. Vernon, *J. Chem. Soc. (Resumed)*, 3293 (1960).
31. E. Atangana, *J. Polym. Environ.*, **27**, 2281 (2019).
32. I. A. Udoetok, R. M. Dimmick, L. D. Wilson and J. V. Headley, *Carbohydr. Polym.*, **136**, 329 (2016).
33. V. Ramos, N. Rodríguez, I. Henning, M. Díaz, M. Monachesi, M.

Rodríguez, A. Abarrategi, V. Correas-Magana, J. Lopez-Lacomba and E. Agullo, *Carbohydr. Polym.*, **64**, 328 (2006).
34. K. S. Sing, *Adv. Colloid Interface Sci.*, **76**, 3 (1998).
35. F. A. Razmi, N. Ngadi, S. Wong, I. M. Inuwa and L. A. Opotu, *J. Clean. Prod.*, **231**, 98 (2019).
36. B. Liu, D. Wang, G. Yu and X. Meng, *Chem. Eng. J.*, **228**, 224 (2013).
37. Y. Lee and W. Lee, *J. Hazard. Mater.*, **178**, 187 (2010).
38. R. R. Mohamed, M. H. A. Elella and M. W. Sabaa, *Int. J. Biol. Macromol.*, **80**, 149 (2015).
39. P. Dadhich, B. Das and S. Dhara, *Carbohydr. Polym.*, **133**, 345 (2015).
40. A. Zuñiga, R. F. Nerán, L. Albertengo and M. S. Rodríguez, *Carbohydr. Polym.*, **202**, 1 (2018).
41. A. Khaleel and B. Dellinger, *Environ. Sci. Technol.*, **36**, 1620 (2002).
42. M. V. Biber and W. Stumm, *Environ. Sci. Technol.*, **28**, 763 (1994).
43. Z. Zong, Y. Kimura, M. Takahashi and H. Yamane, *Polymer*, **41**, 899 (2000).
44. L. Zhirong, M. A. Uddin and S. Zhanxue, *Spectrochim. Acta. A Mol. Biomol. Spectrosc.*, **79**, 1013 (2011).
45. J. Preethi, P. Karthikeyan, S. Vigneshwaran and S. Meenakshi, *Chemosphere*, **262**, 128317 (2021).
46. A. Varrot, C. A. Tarling, J. M. Macdonald, R. V. Stick, D. L. Zechel, S. G. Withers and G. J. Davies, *J. Am. Chem. Soc.*, **125**, 7496 (2003).
47. P. Ma, W. Ding, J. Yuan, L. Yi and H. Zhang, *Environ. Res.*, **184**, 109309 (2020).
48. Y.-S. Ho, *J. Hazard. Mater.*, **136**, 681 (2006).
49. E. S. Dragan, D. Humelnicu, M. V. Dinu and R. I. Olariu, *Chem. Eng. J.*, **330**, 675 (2017).
50. X.-j. Hu, J.-s. Wang, Y.-g. Liu, X. Li, G.-m. Zeng, Z.-l. Bao, X.-x. Zeng, A.-w. Chen and F. Long, *J. Hazard. Mater.*, **185**, 306 (2011).
51. G. Najafpour, *Int. J. Eng.*, **29**, 1319 (2016).
52. S. Hena, *J. Hazard. Mater.*, **181**, 474 (2010).
53. Z. Zhang, X. Wang, H. Wang and J. Zhao, *Chem. Eng. J.*, **344**, 53 (2018).
54. J.-Y. Lin, Y.-L. Chen, X.-Y. Hong, C. Huang and C. Huang, *J. Colloid Interface Sci.*, **561**, 275 (2020).
55. N. A. Ingle, H. V. Dubey, N. Kaur and I. Sharma, *J. Health Res. Rev.*, **1**, 1 (2014).
56. X. Wang, C. Chen, J. Du, X. Tan, D. Xu and S. Yu, *Environ. Sci. Technol.*, **39**, 7084 (2005).
57. T. J. Robshaw, R. Dawson, K. Bonser and M. D. Ogden, *Chem. Eng. J.*, **367**, 149 (2019).
58. A. B. Nasr, C. Charcosset, R. B. Amar and K. Walha, *Desalination Water Treat.*, **54**, 1604 (2015).
59. N. Viswanathan and S. Meenakshi, *J. Hazard. Mater.*, **162**, 920 (2009).
60. Y. Yu, Z. Zhou, Z. Ding, M. Zuo, J. Cheng and C. Jing, *J. Hazard. Mater.*, **377**, 267 (2019).
61. S. Samatya, H. Mizuki, Y. Ito, H. Kawakita and K. Uezu, *React. Funct. Polym.*, **70**, 63 (2010).

Supporting Information

Synthesis and characterization of cross linked N-methylene phosphonic chitosan resin chelated with Al(III) for use as adsorbent for fluoride removal from aqueous solutions

Junyu Fan*, Longhua Yu, Xin Zhou*, and Jie Liu*,†**

*Department of Military Facilities, Army Logistics Academy, Chongqing, 401311, China
**School of Environmental Science and Engineering, Hunan University, Changsha, 410082, China
(*Received 3 June 2021 • Revised 27 July 2021 • Accepted 3 August 2021*)

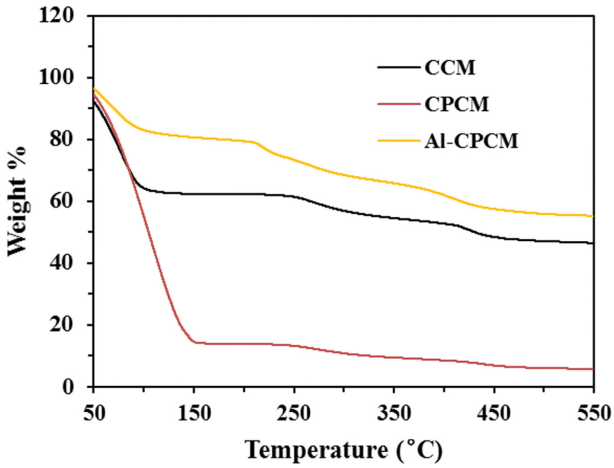

Fig. S1. The TGA weight loss curves of CCM, CPCM and Al-CPCM (The weight loss with increasing temperature of all samples could be divided into three stages. The initial weight losses occurred below 150 °C, which was caused by absorbed water. It can be seen that the water content of MCPC was much higher than that of CCM and Al-CPCM, which was consistent with the results of swelling experiment. The second stage between 200 to 400 °C was related to the destruction of crosslinks and chains of chitosan [1]. The last stage was the temperature was up to 400 °C, and in this stage, the samples were almost decomposed and carbonized.).

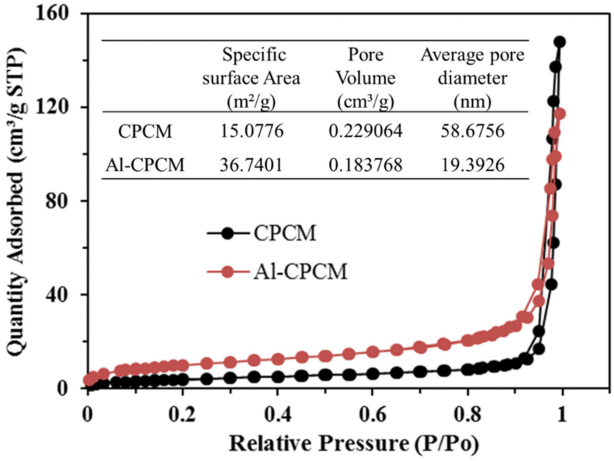

	Specific surface Area (m^2/g)	Pore Volume (cm^3/g)	Average pore diameter (nm)
CPCM	15.0776	0.229064	58.6756
Al-CPCM	36.7401	0.183768	19.3926

Fig. S2. The BET nitrogen adsorption-desorption curves and calculated parameters of CPCM and Al-CPCM.

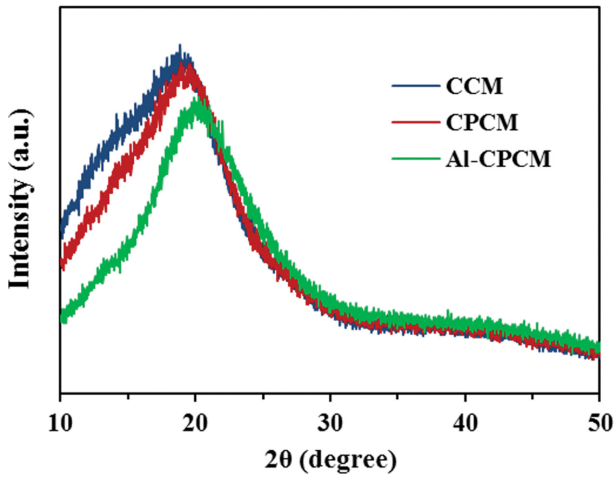

Fig. S3. The XRD patterns of CCM, CPCM and Al-CPCM.

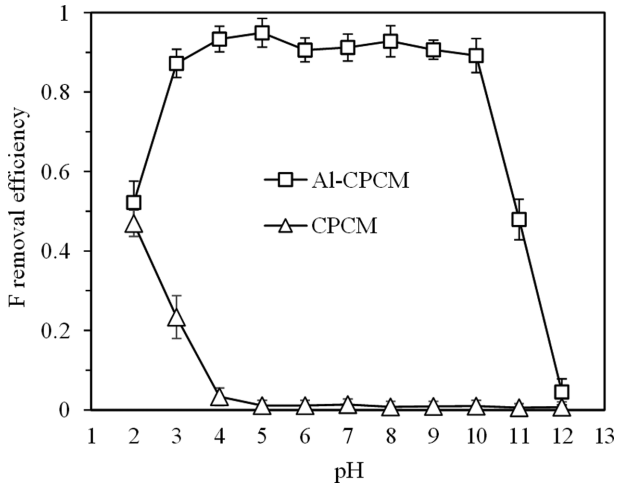

Fig. S4. The pH edge of CPCM and Al-CPCM beads (Experimental conditions: adsorbent dosage: 3 g-wet beads/L; initial concentration of F^-: 20 mg/L; temperature: 25 °C; shaking speed: 220 rpm; contact time: 24 h).

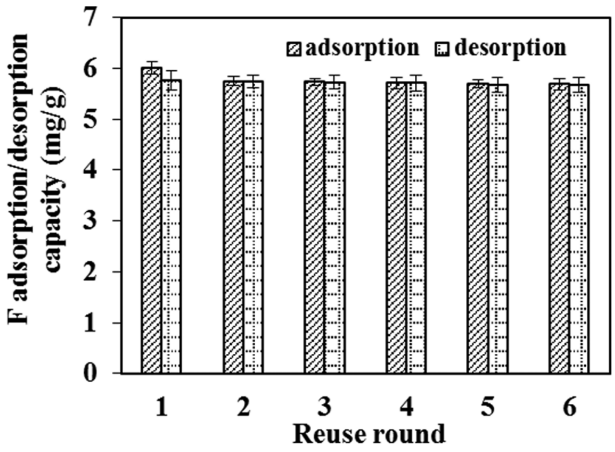

Fig. S5. The adsorption/desorption cycles of fluoride on Al-CPCM resins (Adsorption conditions: adsorbent dosage: 3 g-wet beads/L; initial concentration of F^-: 20 mg/L; initial pH 7; shaking speed: 220 rpm; contact time: 24 h; background: 0.04 M NaCl. Desorption conditions: 1 M $Al_2(SO_4)_3$, 6 h).

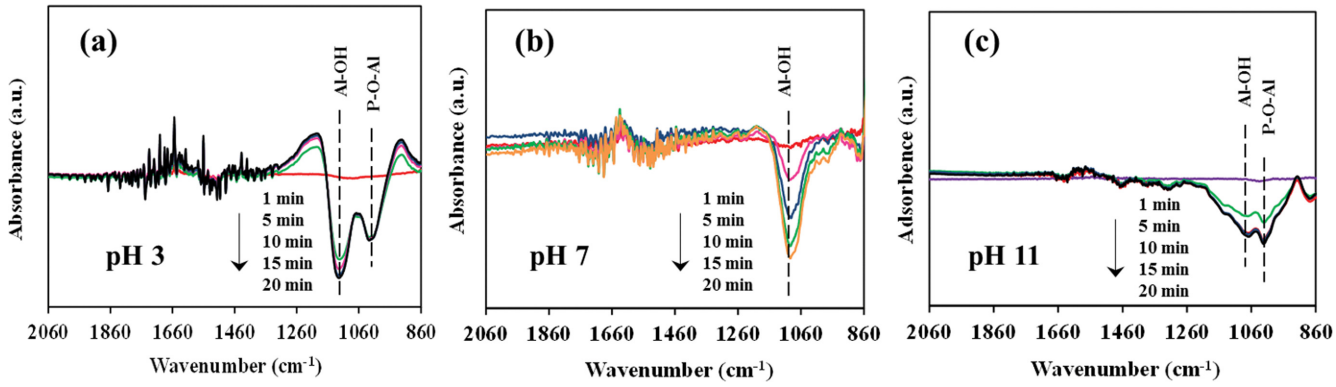

Fig. S6. The in-situ FTIR spectra of Al-CPCM in fluoride solution with different pH.

Table S1. The parameters of actual groundwater sample

	Detection value	Detection method
General parameters		
pH	8.09-8.31	pH electrode
TDS (mg/L)	566-597	TDS probe
Turbidity	0.84-1.17	Scatterometer
Anions		
Fluoride (mg/L)	2.14	ISE probe
Chloride (mg/L)	233.9	IC
Sulfate (mg/L)	18.65	IC
Nitrate (mg/L)	8.84	IC
Bicarbonate (mg/L)	27.3	titration
Phosphate (mg/L)	13.95	IC
Silicate (mg/L)	5.76	IC
Arsenite (μg/L)	3.3	LC-AFS
Arsenate (μg/L)	144.8	LC-AFS
Cations		
Na^+ (mg/L)	295.1	ICP-OES
K^+ (mg/L)	1.14	ICP-OES
Ca^{2+} (mg/L)	16.78	ICP-OES
Mg^{2+} (mg/L)	38.64	ICP-OES
Mn^{2+} (mg/L)	0.57	ICP-OES
Fe^{2+}/Fe^{3+} (mg/L)	BD	ICP-OES
Cu^{2+} (mg/L)	BD	ICP-OES
Cd^{2+} (mg/L)	BD	ICP-OES

Geographic information: 29°48′13″ **N**, 102°52′06″ **E**; Well depth: 20 m.

Table S2. The common peaks assignment of FTIR spectra

Location	Assignment	Ref.
3,500-3,200 cm^{-1}	Stretching vibrations of O-H and N-H in hydroxyl and amino (imino)	[2]
2,930-2,850 cm^{-1}	C-H stretching vibrations in $-CH_2-$ and $-CH_3$	[3]
1,155 cm^{-1}	Glycosides (C-O-C) skeletal vibration	[4]
1,073 and 1,037 cm^{-1}	C-O stretching vibration peaks of hydroxyl on chitosan	[5]
1,631-1,261 cm^{-1}	Stretching and deformation of different amide groups (Amide I, II, III)	[6]

Table S3. The fitting data of column experiment by the Dose-Response model

Flow rate (BV/h)	6		12		24	
	Round 1	Round 2	Round 1	Round 2	Round 1	Round 2
a	6.7706	6.3767	4.1021	3.9152	4.2426	3.9775
b (mg·L/g-dry resin)	204.5296	194.6113	116.5548	108.8418	83.7633	76.8593
q_0 (mg/g-dry resin)	83.3269	79.2861	47.4853	44.3429	34.1258	31.3131
R^2	0.9973	0.9977	0.9951	0.9951	0.9964	0.9953

REFERENCES

1. C. d. T. Neto, J. A. Giacometti, A. E. Job, F. C. Ferreira, J. L. Fonseca and M. R. Pereira, *Carbohydr. Polym.*, **62**, 97 (2005).
2. Q. Li, Q. Mao, M. Li, S. Zhang, G. He and W. Zhang, *Carbohydr. Polym.*, **234**, 115926 (2020).
3. B. Geng, Z. Jin, T. Li and X. Qi, *Sci. Total. Environ.*, **407**, 4994 (2009).
4. J. Preethi, P. Karthikeyan, S. Vigneshwaran and S. Meenakshi, *Chemosphere*, **262**, 128317 (2021).
5. E. Guibal, C. Milot, O. Eterradossi, C. Gauffier and A. Domard, *Int. J. Biol. Macromol.*, **24**, 49 (1999).
6. Y. Xie, S. Li, F. Wang and G. Liu, *Chem. Eng. J.*, **156**, 56 (2010).